Polarization Relaxation in an Ionic Liquid Confined between Electrified Walls †

ARTICLE *in* THE JOURNAL OF PHYSICAL CHEMISTRY B · JUNE 2007

Impact Factor: 3.3 · DOI: 10.1021/jp067184+ · Source: PubMed

4 AUTHORS, INCLUDING:

Carlos Pinilla
University College London
22 PUBLICATIONS **531** CITATIONS
SEE PROFILE

R. M. Lynden-Bell
University of Cambridge
205 PUBLICATIONS **7,514** CITATIONS
SEE PROFILE

Polarization Relaxation in an Ionic Liquid Confined between Electrified Walls†

Carlos Pinilla,‡ M. G. Del Pópolo,‡ Jorge Kohanoff,‡ and R. M. Lynden-Bell‡,§,*

Atomistic Simulation Centre, School of Mathematics and Physics, Queen's University Belfast, BT7 1NN, U.K., and University Chemical Laboratory, Lensfield Road, Cambridge University, Cambridge CB2 1EW, U.K.

Received: October 31, 2006; In Final Form: December 30, 2006

The response of a room temperature molten salt to an external electric field when it is confined to a nanoslit is studied by molecular dynamics simulations. The fluid is confined between two parallel and oppositely charged walls, emulating two electrified solid−liquid interfaces. Attention is focused on structural, electrostatic, and dynamical properties, which are compared with those of the nonpolarized fluid. It is found that the relaxation of the electrostatic potential, after switching the electric field off, occurs in two stages. A first, subpicosecond process accounts for 80% of the decay and is followed by a second subdiffusive process with a time constant of 8 ps. Diffusion is not involved in the relaxation, which is mostly driven by small anion translations. The relaxation of the polarization in the confined system is discussed in terms of the spectrum of charge density fluctuations in the bulk.

1. Introduction

Room temperature ionic liquids (RTILs) have attracted a lot of attention in recent years due to a wide range of potential applications in electrochemical systems, such as lithium batteries,[1] double layer capacitors,[2] fuel cells[2] and solar cells.[3] As is well-established experimentally, a low-temperature molten salt is obtained by combining large organic cations with different anions to produce fluids with varying physicochemical properties. Large molecular volumes and a subtle competition between van der Waals and Coulombic forces result in frustrated ionic packing that prevents crystallization at room temperature.

Considering the relevance of ionic liquids in electrochemical contexts, it is important to gain insight into their behavior when subject to external electric fields. Electrochemical interfaces involving aqueous electrolytes[4−6] or even simple molten salts[7−9] have been substantially investigated in the past; however, it is not clear to what extent the understanding gained from these systems applies to organic molten salts, which exhibit complex interactions and orientational degrees of freedom. One may conjecture, for example, that ionic liquids based on dissimilar cations may lead to different local structures near cathodes and anodes, affecting, for example, interfacial electron- and ion-transfer reactions.[10,11]

A well-documented application of ionic liquids is their use as support electrolytes in dye-sensitized solar cells (DSSCs).[12] DSSCs are photovoltaic devices consisting of a layer of nanoporous TiO_2, coated with a light-sensitive dye, clamped between two metallic electrodes. The interstices left between the TiO_2 grains are filled with a liquid electrolyte that dissolves a redox couple (usually I^-/I_3^-). Under illumination, electrons are transferred from the dye to the conduction band of the semiconductor. The oxidized dye is subsequently reduced by the redox couple, which is in turn regenerated at the counter electrode. Ionic liquids, in particular those based on 1,3-dialkylmidazolium cations, have been extensively tested in such devices[12] for several reasons. They are liquid at room temperature and can conduct an electric current; they exhibit low degradation and evaporation rates, they have a high viscosity that prevents leaking;[13] and most importantly, they display a fast and efficient screening of electric fields. In fact, it appears that despite the high viscosity of the molten salt, the screening of the charge injected into the TiO_2 nanoparticles is achieved very quickly (in less than 1 ps) so that this process is one of the fastest of the many kinetic bottlenecks in an operating DSSC.[14−18] To our knowledge, the only computational work aiming at understanding dynamic screening at the solid/molten-salt interface is the study of Lanning and Madden.[19] This is based on a model of spherical ions as a first approximation to the description of the functioning of dye-sensitized solar cells.

In a previous article,[20] we considered the behavior of the ionic liquid dimethylimidazolium chloride, [dmim][Cl], confined between two parallel noncorrugated walls as a function of wall separation, from 2.5 to 4.5 nm. Changes in structural and dynamical properties were studied as a function of the interwall separation. Here, we extend our previous investigation by focusing on structural and kinetic effects induced by a uniform electric field perpendicular to the confining walls. The aim is to model the behavior of the fluid trapped within the porous network of a DSSC,[21] where the pore size is ∼4 nm.[24]

The present paper is organized as follows: methodology and computational details are described in Section 2. In Section 3, structural and dynamical properties of [dmim][Cl] confined between two walls, in the presence and absence of an electric field, are discussed. A more general discussion and our conclusions are presented in Sections 4 and 5, respectively.

2. Methodology and Computational Methods

The $[dmim]^+$ cation, shown in Figure 1, was treated as a rigid 10-site molecule with united methyl groups. Partial charges were assigned to atomic sites according to the values reported by Hanke et al.,[22] whereas dispersion interactions were modeled by Lennard−Jones potentials using the parameters reported by de Andrade et al.[23]

The setup is illustrated in Figure 2. Five hundred and four ion pairs were placed in a rectangular box surrounded by

† Part of the special issue "Physical Chemistry of Ionic Liquids".

* Corresponding author. Tel: +44 (1223) 336535. E-mail: rmlb@cam.ac.uk.

‡ Queen's University Belfast.

§ Cambridge University.

10.1021/jp067184+ CCC: $37.00
Published on Web 02/13/2007

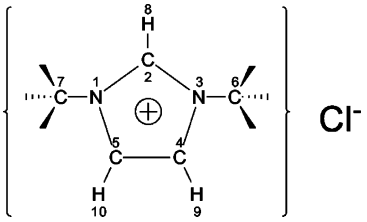

Figure 1. Dimethylimidazolium chloride, [dmim][Cl]. A rigid, 10-site model with united methyl groups was used in the simulations.

periodic images. Molecules were confined to a slit by two parallel structureless walls (71 Å × 41 Å), located perpendicular to the principal or *z*-axis of the cell (lying horizontally in the figure) and separated by a distance of $D = 44.9$ Å. This distance was chosen according to the estimated spacing between dye-coated nanoparticles in a dye-sensitized solar cell.[24] Periodic images were applied in the plane of the slit to give a semi-infinite slab and in the direction perpendicular to the slit at 110 Å to give a system of replicated parallel infinite slabs separated by a slab of vacuum.

The interaction between the molecules and the walls was modeled by an integrated Lennard−Jones potential of the form[25]

$$V_{\text{wall}}(z) = \frac{2\pi\sigma_{\text{w}}^{3}\epsilon_{\text{w}}\rho}{3}\left\{\frac{2}{15}\left(\frac{\sigma_{\text{w}}}{z}\right)^{9} - \left(\frac{\sigma_{\text{w}}}{z}\right)^{3}\right\} \quad (1)$$

where $\sigma_{\text{w}} = 3.0$ Å, $\epsilon_{\text{w}} = 0.8$ kJ/mol, and $4\pi\rho = 0.5$ sites/Å.[3] These values are based on those for silica. $V_{\text{wall}}(z)$ was combined with the atomic Lennard−Jones potentials using Lorentz−Berthelot mixing rules ($\sigma_{ij} = 0.5(\sigma_{ii} + \sigma_{jj})$ and $\epsilon_{ij} = (\epsilon_{ii}\epsilon_{jj})^{1/2}$).

The external electric field corresponded to that provided by equal and opposite uniform charge distributions on the surfaces of the two walls,[26]

$$E_z = \frac{\sigma}{\epsilon_0} \quad (2)$$

where σ is the surface charge density and ϵ_0 is the vacuum permittivity. This field results in an extra force F_i on each charged site i in the system,

$$F_{i,z} = \frac{q_i\sigma}{\epsilon_0} \quad (3)$$

where q_i is the charge on the ith site.

Molecular dynamics (MD) simulations where performed with a time step of 2 fs in the canonical ensemble using a Berendsen thermostat. The simulations were performed with a modified version of the DL_POLY code.[27]

Strictly speaking, the confined system should be periodic only in the directions parallel to the walls, and the electrostatic interactions should be calculated using a 2-D method; however, the 2-D Ewald method is considerably more expensive than 3-D Ewald sums. Consequently, the electrostatic interactions were calculated with regular 3-D Ewald sums[28] using a real space cutoff of 20 Å but emulating a semi-infinite slab geometry by leaving a vacuum space of 65 Å between the two confining walls along the *z* direction (see Figure 2).

A difficulty with this setup is that the sample dipole moment, induced by the external field, may lead to a nonnegligible interaction between neighboring cells along *z*. Such an interaction could result on a sizable dependence of the observables on the interslab distance. To mitigate this problem, the Yeh and Berkowitz correction[29] was implemented and tested. Several highly polarized configurations were selected, and the forces on the particles were compared with those resulting from a rigorous 2-D Ewald sum. For the highest electric field considered here, the maximum difference in forces never exceeded 5%.

MD simulations were run for a value of σ of 2 μC/cm^2 (2×10^{-2} C/m^2 or 0.001 248 e/Å^2), equivalent to the estimated surface charge densities of TiO_2 under full illumination.[30−32] Eight independent trajectories were run for the system with both charged and uncharged walls. Each of the eight simulations was equilibrated for 600 ps at temperatures of 1000, 800, 600, and 400 K before collecting data during production runs of 800 ps at the final temperature. One trajectory was extended to 1.5 ns, and no further structural changes were seen. These runs (with a total length of 7.1 ns for charged and 6.4 ns for uncharged systems) were the basis of the analysis of the behavior of [dmim][Cl] in a static electric field. Subsequently, for 15 independent configurations of the system with $\sigma = 2.0$ μC/cm^2, the field was switched off, and the evolution of the system was followed for 100 ps in the microcanonical ensemble. Error bars were calculated from the standard deviations of the means of independent trajectories.

3. Results

3.1. Structural Properties of [dmim][Cl] in an External Electric Field. Figure 3a shows the local density of cations and anions for [dmim][Cl] confined between two parallel walls in the absence of electric field. The layering pattern and other structural features of this nonpolarized system were reported previously.[20] Figure 3b shows the center-of-mass densities of cations and anions along the confinement axis in the presence of the electric field ($E = 2.25$ 10^9 V/m). As expected, charge displacement results in a net polarization of the liquid that tries to balance the external field. The density profiles show that, with respect to the nonperturbed fluid, anions redistribute more than cations, and such changes occur mainly within the first two layers closer to the walls. Such structural changes are confined to a region ∼7.0 Å wide near the electrodes, in line with the experimental observations of Baldelli[33] on a [bmim][BF_4]/Pt interface. From Figure 3b, it is also clear that, as a consequence of the different size and shape of the ions, the interface reacts differently to a positive or a negative polarization. It seems that, as small spherical objects, chlorides can approach the positive electrode more easily than the [dmim]$^+$ molecules can translate or reorient at the other electrode. At the positive wall, anions are segregated toward the surface, whereas on the negative wall, both ions coexist in the same layer. Interestingly, the first two layers of anions near the negative wall are much sharper than in the unperturbed fluid, a feature that develops systematically on increasing polarization. Such effect results in a rather unexpected behavior. Contrary to what would happen in a dilute electrolyte solution in which the size and shape of the ions is not important, there is no significant accumulation of cations near the negatively charged wall. Rather, the smaller anions are repelled by the negative charge in the wall and move toward the interior of the slab.

Figure 4a and b shows the average electrostatic potential along the confinement axis for the fluid in the presence of an electric field. The potential was found by integrating the Poisson equation,

$$\Phi(z)_l = -\frac{1}{\epsilon_0}\int_{-b}^{z}(z - z')\rho_q(z')\,\mathrm{d}z' \quad (4)$$

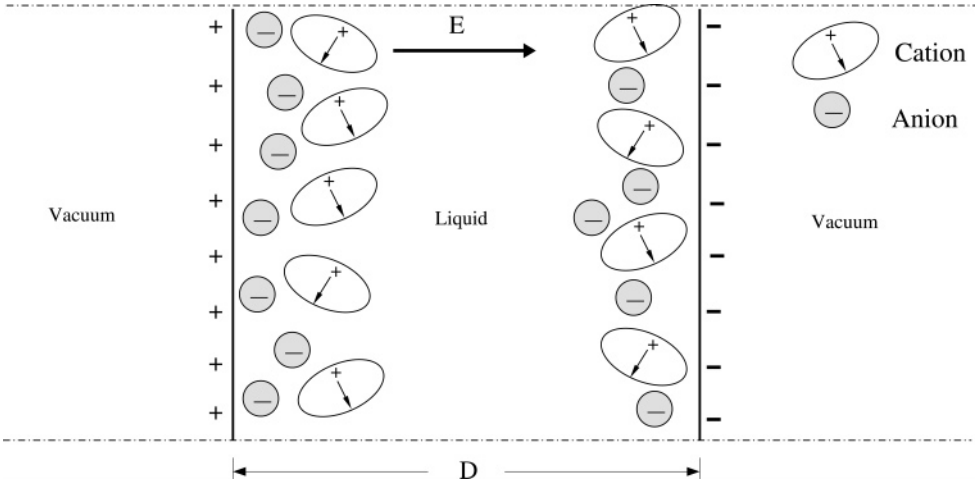

Figure 2. Schematic representation of the simulation cell with the *z* direction horizontal. The liquid is confined between the two electrified walls separated by 44.9 Å, and periodic boundaries are applied in the *x* and *y* directions (at the top and bottom of the figure). The region outside is vacuum. The system is periodically repeated every 110 Å in the *z* direction. The arrow in the cations represents a vector perpendicular to the imidazolium ring, forming an average angle of 70° with respect to the surface normal, as is found on average near the walls.

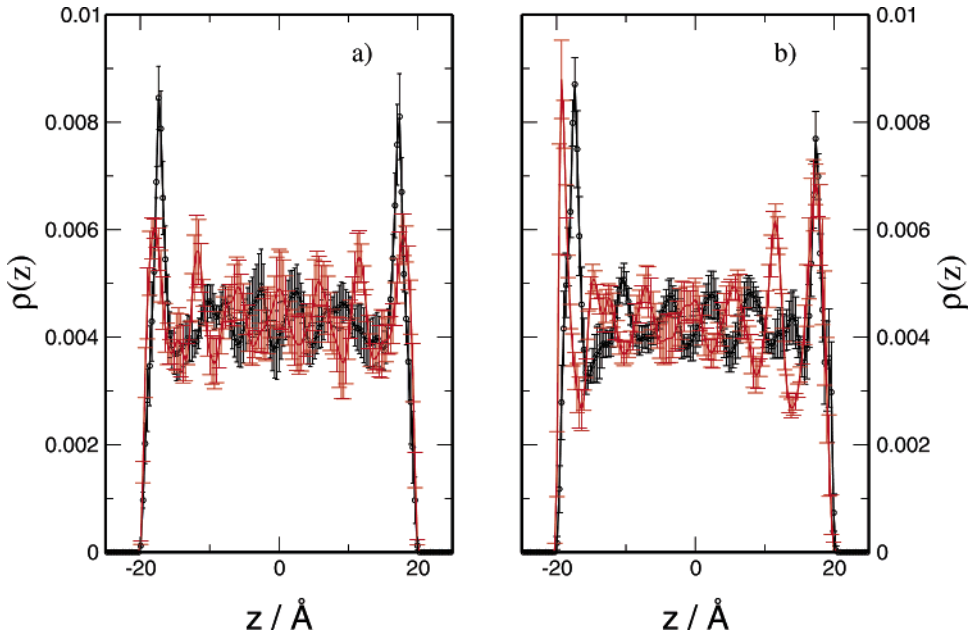

Figure 3. Ion number density profiles for $[dmim]^+$ (black line) and Cl^- (red line) confined between two parallel walls separated by 44.9 Å. Plots a and b correspond respectively to the system without and with an external electric field generated by a uniform surface charge density, σ, of 2.0 $\mu C/cm^2$. The left wall has a positive charge.

where $\rho_q(z')$ is the average charge density in a slice of liquid at position z' along the axis perpendicular to the walls, and $-b$ is the position of the left wall ($b = 20$ Å in the present case). This integral represents the potential due to the fluid and does not include the external potential due to the walls because the integral does not include the charge on the walls. The charge density $\rho_q(z)$ (calculated from the atomic charges) is shown in the inset of Figure 4b. Figure 4a shows the potential due to the liquid, $\Phi_l(z)$, that is, the solution of eq 4. The dashed straight line in Figure 4a is (minus) the bare potential of the external field $-\Phi_e(z)$, showing that the response of the liquid is to establish a compensating potential so as to screen the external field. The extent of the screening is shown in Figure 4b, which shows the total electrostatic potential in the confinement region, $\Phi_t(z) = \Phi_l(z) + \Phi_e(z)$ with and without the external field. Clearly, there is a total potential drop across the cell of ~0.35 V, resulting in an overall capacitance of 35 times that of the empty system, C_{vac}. If the separation between the walls were sufficiently large, a constant potential would be reached at the center of the region, and the capacitance would be written as the sum of the capacitances of the double layers at the cathode and anode.

$$C^{-1} = C_{an}{}^{-1} + C_{cat}{}^{-1} \tag{5}$$

In the present case, relevant for dye-sensitized solar cells, the separation between walls is not large enough for bulk behavior to be reached at the center of the cell, and it is not possible to separate the capacitance of the two interfaces.

It is also interesting to look for possible changes in the molecular orientations induced by the external field, bearing in mind that such structural details may play a role in charge-transfer processes at the interface.[10,11] The orientational structure through the liquid slab can be analyzed in terms of order parameters $P_2(\cos\theta) = \langle(3\cos^2\theta - 1)/2\rangle$, where θ is the angle between a vector fixed to the cation frame and a vector

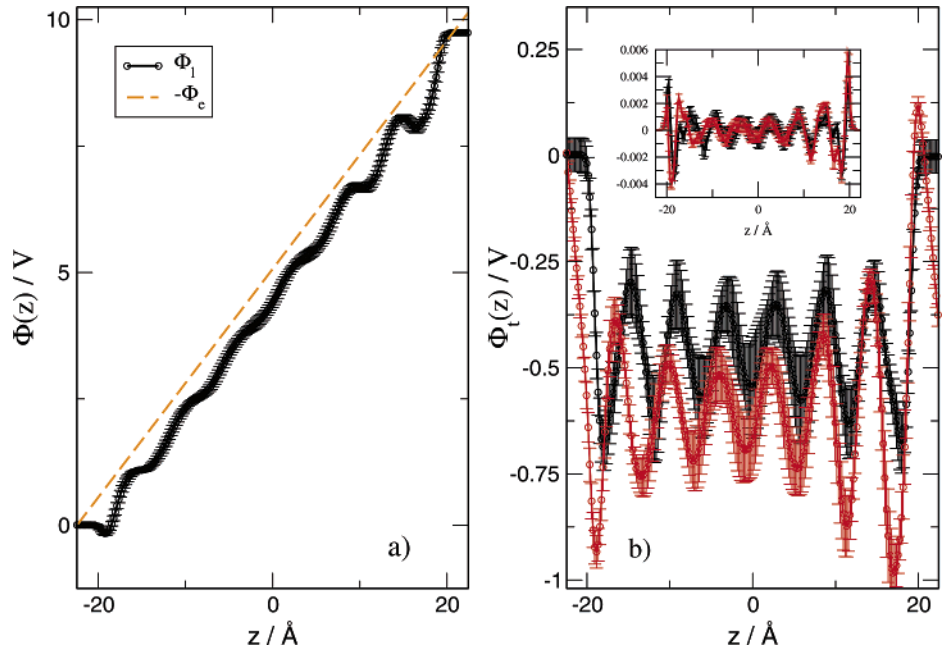

Figure 4. Electrostatic potential profiles (in V) along the confinement axis (z) resulting from the solution of eq 4. In panel a, the dashed line is (minus) the external electrostatic potential, Φ_e, whereas the bold line is the potential due to the liquid, Φ_l. In panel b, the red line depicts the total potential $\Phi_l + \Phi_e$, along the liquid slab, whereas the black line corresponds to the electrostatic potential for a system without external field. The inset of part b shows the charge densities for the system with (red line) and without (black line) an external field.

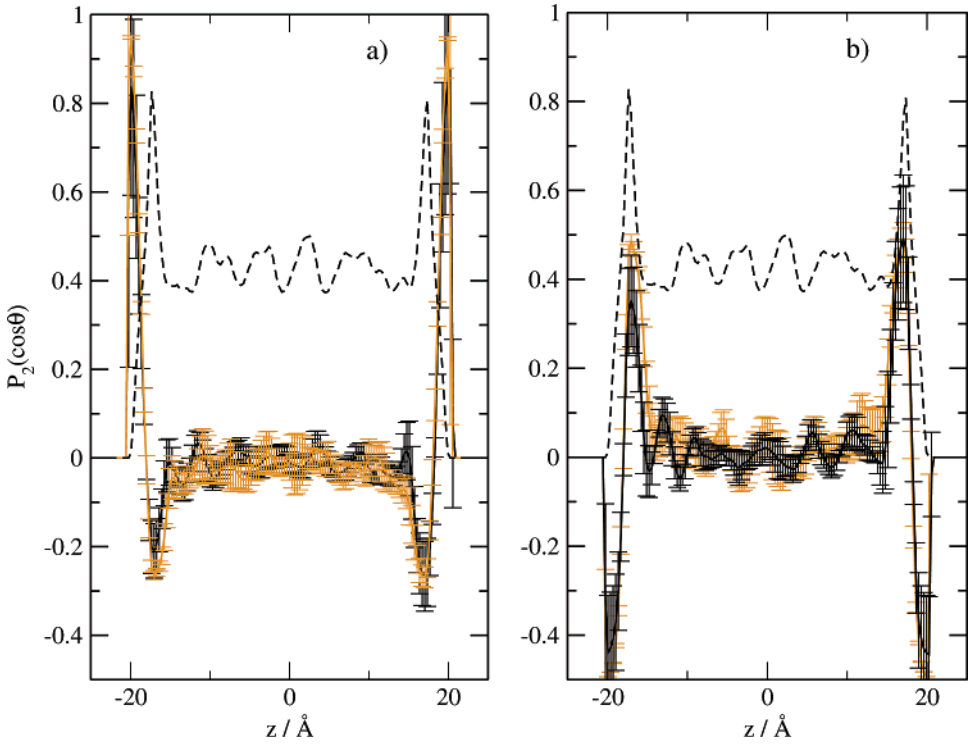

Figure 5. Orientational-order parameter $P_2(z)$ along the confinement axis for the polarized (black line) and nonpolarized (orange line) systems. The dashed line shows the (scaled) cation density profile for reference. Panel a shows the orientation of an axis perpendicular to the cation plane. Panel b gives the orientation of an axis connecting the two nitrogen atoms in the cation ring.

perpendicular to the walls (along z). The brackets represent an average over molecules at position z and over different configurations. Figure 5 shows the variation of $P_2(\cos\theta)$ as a function of z for (a) a vector normal to the cation plane ($\theta_\perp$) and (b) a vector joining the two nitrogen atoms (θ_{NN}). The P_2 profiles are shown for the polarized and unpolarized liquid, and a scaled density profile is provided as a reference.

In the unpolarized system, there are a few cations very close to the surface which lie flat on the surface ($P_2(\cos\theta_\perp)$ near 1 and $P_2(\cos\theta_{NN})$ near -0.5). However, most of the cations in the first layer are oriented at an angle to the surface, with $P_2(\cos\theta_\perp)$ negative and $P_2(\cos\theta_{NN})$ positive. This corresponds to the cations being preferentially aligned with their NN axes toward the surface normal and their rings perpendicular to the surface plane. The average tilt of the cation rings is $\sim 70°$ with respect to the surface plane.

At the charge levels relevant to dye-sensitized solar cells and used in these simulations, the effect of charging the walls on

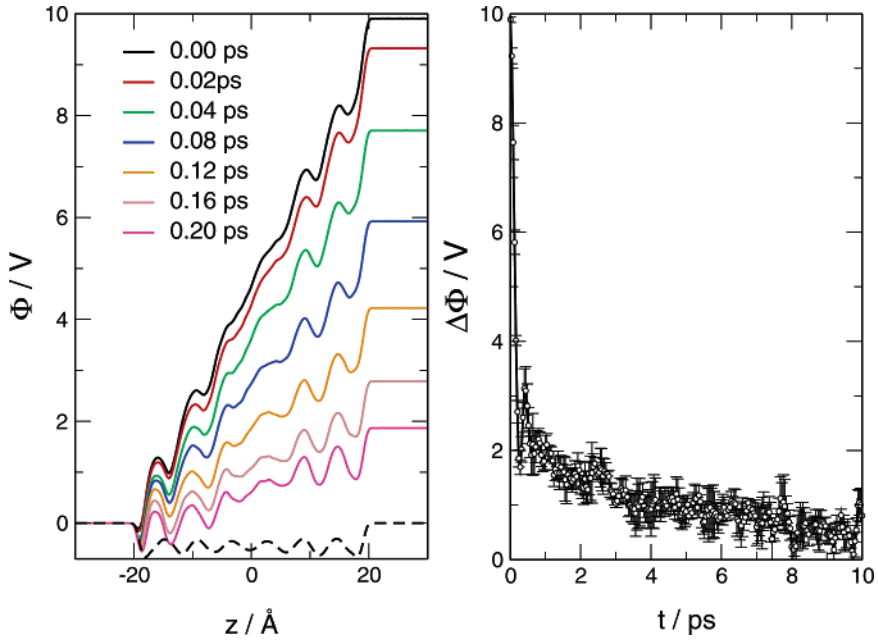

Figure 6. Electrostatic potential relaxation: (a) Electrostatic potential profile along the confinement axis for different times after the electric field was switched off ($t = 0$ ps). (b) Electrostatic potential difference ($\Delta\Phi$) between the two electrodes as a function of time (with error bars).

the cation orientation is small. Any changes at the negative wall are less than the error bars, whereas in the first layer near the positive wall, the cation rings are slightly more perpendicular to the walls.

Finally, to explore whether the polarization induced along the *z*-axis is accompanied by structural changes in the plane parallel to the walls, planar radial distribution functions, $g(r)$, were calculated for r vectors lying on the $X-Y$ plane. The results (not reported in this paper) showed no significant differences in the contact layers between the systems with and without the electric field.

These results suggest a picture of the electrified [dmim][Cl]/solid interface as sketched in Figure 2. Anions segregate significantly toward the positive electrode, while on the negative side, both ions coexist in the same layer. Cations rearrange slightly, and their orientation remains similar to that in the nonpolarized system.

3.2. Relaxation of the Electrostatic Potential. To study the relaxation dynamics, the external field was switched off, and the decay of the potential in the liquid, Φ_l, was monitored as a function of time. Fifteen different trajectories were used, starting from independent initial configurations. Figure 6a shows $\Phi_l(z, t)$ at different times after the electric field was turned off ($t = 0$). Each curve corresponds to an average over trajectories. Figure 6b shows the potential difference ($\Delta\Phi$) between the two electrodes as a function of time. Overall, the relaxation process is characterized by two regimes: a fast process, occurring in <0.2 ps, that accounts for a potential drop of 80%; and a second slower process with a characteristic time of 8 ps.

To distinguish which degrees of freedom participate most in the relaxation, the time evolution of the electric current $j(t)$ (the time derivative of the polarization), was divided into cation and anion contributions

$$j(t) = \sum_{i=1}^{N_{cat}} \sum_{j=1}^{M_{at}} q_i^j \dot{z}_i^j(t) + \sum_{i=1}^{N_{an}} q_i \dot{z}_i(t) \qquad (6)$$

where the sums run over atoms and molecules, N_{cat} and N_{an} are the number of cations and anions, respectively; M_{at} is the number of atoms in a cation; q_i is the charge of the ith particle; and $\dot{z}_i$ its velocity along the *z*-axis. Figure 7 shows the evolution of the former quantities as a function of time after switching off the external field. The blue line corresponds to $j(t)$, and the other two lines, to anions and cations, respectively. It is quite clear that anions dominate the discharge current during the whole transient but, most importantly, during the subpicosecond process.

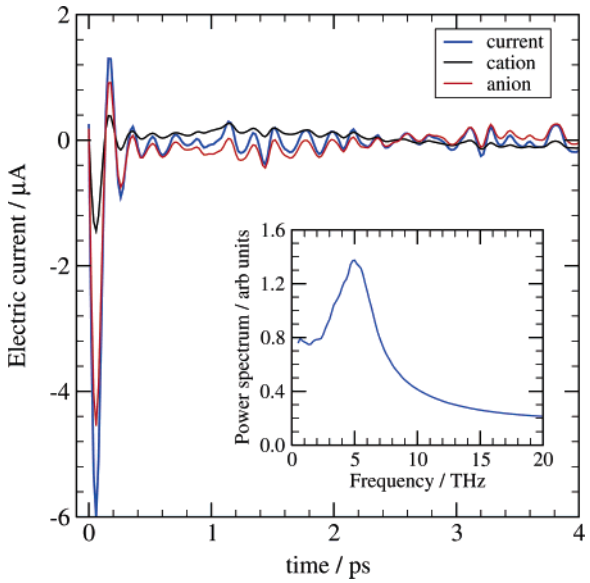

Figure 7. Discharge current $j(t)$ (blue line) and its decomposition into anion (red) and cation (black) contributions. Inset: Fourier transform of the total current.

The two partial currents have the same sign, since cations and anions move in opposite directions. However, their magnitude is quite different. After this initial oscillation, the cationic current becomes negligible, while the rest of the discharge is driven by the anions, but at significantly lower levels than during the initial, subpicosecond process. Finally, the inset to Figure 7 shows the Fourier transform of $j(t)$, exhibiting a clear

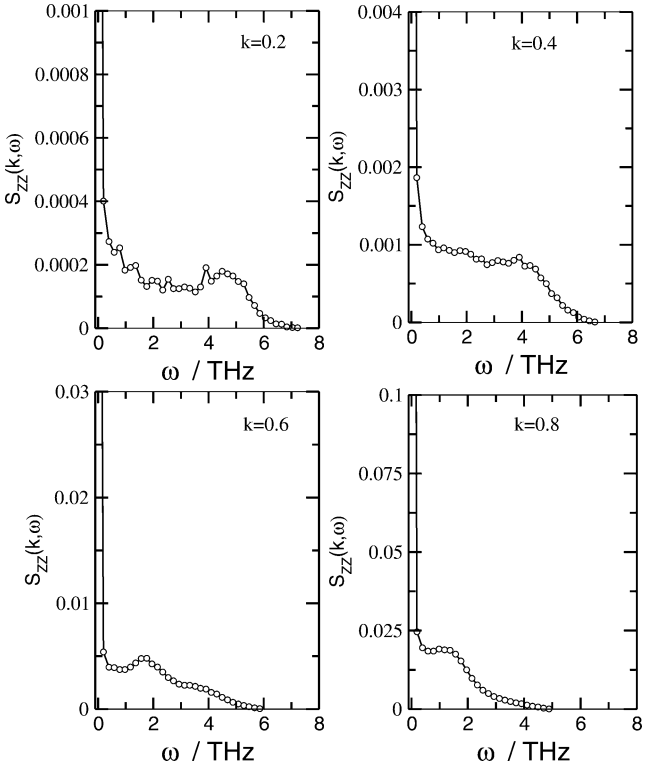

Figure 8. Calculated dynamic structure factor, $S_{ZZ}(k, \omega)$, for bulk [dmim][Cl] at 400 K at various values of k.

maximum at a frequency of ~5 ps^{-1} (5 THz). This suggests a dynamics characterized by a damped plasmalike oscillation.

It is important to stress that the time scales reported above are well below those associated with structural relaxation in imidazolium-based ionic liquids, which are on the order of hundreds of picoseconds.[35−38] This shows that the relaxation of the electrostatic potential does not involve ionic diffusion over long distances, but rather, a small relative motion of cations and anions, mostly in the highly polarized regions near the electrodes. In the next subsection, it will be shown that, for confined [dmim][Cl], the electrostatic potential relaxation follows a dynamics similar to that of a high-frequency and long-wavelength excitation of the charge density in the bulk (a damped plasmalike oscillation).

3.3. Equilibrium Charge Density Fluctuations in Bulk [dmim][Cl]. A complete characterization of equilibrium charge density fluctuations in a homogeneous ionic fluid is given by the charge−charge dynamical structure factor,[39]

$$S_{ZZ}(\mathbf{k}, \omega) = \frac{1}{2\pi}\int_{-\infty}^{+\infty} F_{ZZ}(\mathbf{k}, t)\mathrm{e}^{-i\omega t}\,\mathrm{d}t \qquad (7)$$

where $F_{ZZ}(\mathbf{k}, t) = (1/N)\langle\rho_{\mathbf{k}}(t)\rho_{-\mathbf{k}}(0)\rangle$ is the time correlation function for a charge density modulation of wave vector $\mathbf{k}$,

$$\rho_{\mathbf{k}}(t) = \sum_{i=1}^{N} q_i \mathrm{e}^{-i\mathbf{k}\cdot\mathbf{r}_i(t)} \qquad (8)$$

in a system of N particles carrying charges q_i located at positions $\mathbf{r}_i(t)$.

Figure 8 shows $S_{ZZ}(k, \omega)$ for bulk [dmim][Cl] at 400 K calculated at $|\mathbf{k}| = k = 0.2$, 0.4, 0.6, and 0.8 Å^{-1} (see reference 40 for a similar study of [bmim][Cl]). As a function of ω, $S_{ZZ}(k, \omega)$ exhibits a well-defined peak that shifts to higher frequencies for increasing wavelengths. Such dispersive behavior resembles that of a longitudinal optic-type mode (LO) in ionic crystals in which cations and anions move out of phase and is represented by the squares in Figure 9. In the same figure, the line with circles corresponds to an approximation to the frequency of the LO mode, ω_{LO}, based on a short time expansion of $F_{ZZ}(\mathbf{k}, t)$,[41]

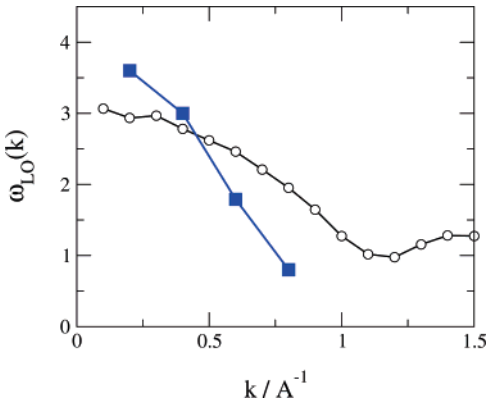

Figure 9. Blue squares: k-dependence of the frequency, $\omega(k)$, at which the maxima of $S_{ZZ}(k,\omega)$ are observed in Figure 8. Circles: $\omega_{LO}(k)$ calculated using eq 9.

$$[\omega_{LO}(\mathbf{k})]^4 = \frac{\langle\omega^4 S(\mathbf{k}, \omega)\rangle}{S(\mathbf{k})} \qquad (9)$$

where $\langle\omega^4 S(\mathbf{k}, \omega)\rangle$ is the fourth moment of $S_{ZZ}(\mathbf{k},\omega)$, calculated from the simulations as

$$\langle\omega^4 S\rangle = \frac{1}{N}\langle\ddot{\rho}_{\mathbf{k}}(0)\,\ddot{\rho}_{\mathbf{k}}(0)\rangle \qquad (10)$$

The "plasma" frequency, ω_p, is defined as $\omega_p = \lim_{k\to 0}\omega_{LO}(k)$. In Figure 9, a simple eye-guided extrapolation to $k = 0$ leads to similar estimates of ω_p for both approaches, that is, ω_p between 3.0 and 4.5 THz. These values are in line with the characteristic frequency of 5 THz shown in the inset to Figure 7, which was estimated from nonequilibrium simulations.

The decay of such long-wavelength charge density oscillation in the bulk can be seen more clearly from the various $F_{ZZ}(k, t)$'s, shown in Figure 10. This figure also includes the relaxation of the electrostatic potential, $\Delta\Phi(t)$ (the same as in Figure 6), for comparison. At $k = 1.2$ Å^{-1}, corresponding to the main peak of the structure factor $S_{ZZ}(k)$, the relaxation time is of the order of 200 ps, which is typical of structural rearrangements associated with diffusive behavior. Subsequently, for decreasing k, the behavior of $F_{ZZ}(k, t)$ after the initial process systematically approaches that of $\Delta\Phi(t)$. Clearly, the relaxation of the electrostatic potential in the confined system after switching off the external field strongly resembles the relaxation of a long-wavelength LO mode in the bulk liquid.

4. Discussion

The behavior of ionic liquids near charged surfaces differs from that of dilute electrolytes. In the latter case, the size and shape of the ions is comparatively unimportant, and they can be considered as point charges as a first approximation, with size effects a secondary consideration. This leads to the well-known description in terms of Helmholtz and diffuse double layers. In an ionic liquid or a molten salt, the ions are in contact so that their sizes and shapes are of primary importance. This leads to charge oscillations that may penetrate quite deeply into the liquid, as has been shown by Lanning and Madden for simple, inorganic molten salts.[19] In our earlier work, we showed

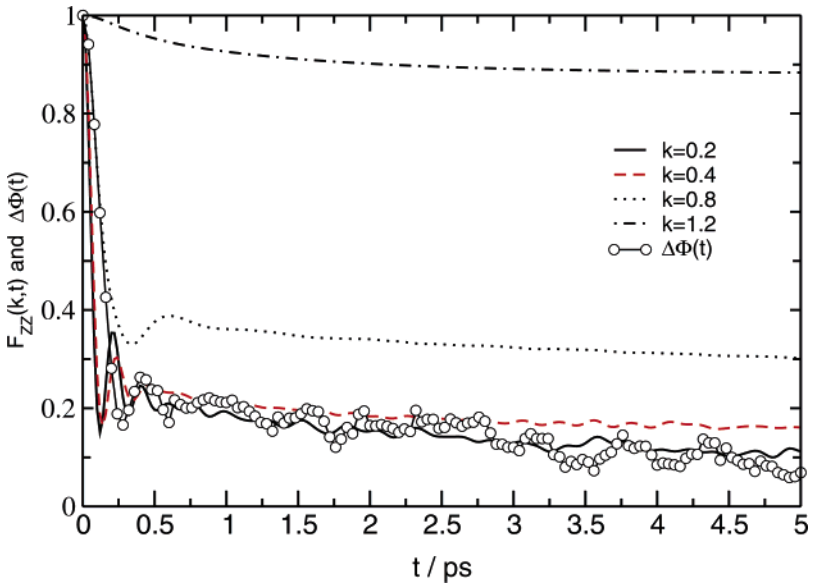

Figure 10. Charge−charge intermediate scattering function $F_{ZZ}(k, t)$, for bulk [dmim][Cl] at 400 K at various values of k. $\Delta\Phi(t)$, electrostatic potential difference between the two electrodes (see Figure 6).

that such layering occurs in [dmim][Cl] confined to nanoscale slits and that the slit would have to be much wider before the liquid showed bulklike behavior near the center.[20] The orientation of the cations near the uncharged surfaces is the result of balancing the energy advantages of good packing with the entropic advantages of random orientations.

Although it is surprising at first sight that the response of the structure to an external field is small (see Figures 3 and 5), the effective screening of the external field is large (see Figure 4). This shows that screening can be achieved by small relative changes in cation and anion positions. Because the cation charge is distributed over the whole molecule with a dipole moment of +1.2 D relative to the center of mass, an isolated cation with its center of mass held at the center of the slit would tend to align with its unique CH group pointing away from the positively charged surface, whereas if it were free to move, it would crash into the negative electrode, where it would lie flat. The observation that in these liquids the orientation of the cations near the charged surfaces is very similar to that near the uncharged surfaces shows that the orientational preference of cations is still dominated by packing and entropic effects under the conditions of the simulation. We would, however, expect to see changes in the orientational distributions at higher field strengths, possibly those found in electrochemical experiments.[33] However, in the latter case, the atomic structure of the electrode surface is also likely to affect the details of the response to an applied field.

The dynamics of the response to an applied field also reflects the fact that the field can be screened by small relative motions of cations and anions, which can occur quickly. This was observed by Lanning and Madden in a simulation of the screening of an electrified surface by molten KCl (1300 K).[19] These authors reported a single exponential and nondiffusive relaxation of the internal potential after removing the electric field. It was proposed that the relaxation mechanism was similar to that of short wavelength, charge-density oscillations in the bulk. We have found much the same behavior in the case of [dmim][Cl], although the relaxation has two time scales (see Figure 6), both of which are still much shorter than the structural relaxation time. By studying the dynamic structure factor (see Figure 8) and the contribution of anions and cations to the discharge current (see Figure 7), we have shown that long-wavelength structure factors decay in a way similar to the potential relaxation and that the anion contribution is several times greater than the cation contribution.

In this simulation, we have used a model with structureless walls and rigid nonpolarizable ions. The details of the dynamic and structural features discussed here are expected to depend on the chemical nature of both the molten salt and the solid.[34] The aim of the present study is to obtain a general description of the behavior of a confined ionic liquid and to analyze the factors that should be considered in their description. The asymmetric response of the fluid near positively and negatively charged surfaces is likely to occur in any ionic liquid in which the ions are of different shapes and sizes. The fast time scale of the response to an applied field is also likely to occur for fields of size comparable to those studied here.

The numerical values of the time scales depend on the ionic liquid and on the model used for its description. We have used a rigid, united atom nonpolarizable model for the cations and a nonpolarizable model for the anions. Youngs[42] has shown that replacing the united atom model for $[dmim]^+$ with one with explicit methyl groups changes the diffusion constant by ∼10%. However, the diffusion constants obtained from simulations of related compounds with nonpolarizable models are low as compared with experiment, and Yan et al.[43] have shown that diffusion rates increase when polarizability is included. We believe that the short time scales of the response and its description in terms of small relative motions of cations and anions would occur in a more realistic model but that the numerical values of the time constants would differ.

5. Conclusions

A liquid slab of dimethylimidazolium chloride confined between two charged solid surfaces in the presence and absence of an electric field was studied by molecular dynamics simulations. For increasing field strengths, a systematic rearrangement of the ions, mainly due to anion segregation toward the positive electrode and away from the negative wall, is the most noticeable structural change. The resulting potential drop between the two electrodes is ∼0.35 V, leading to an overall capacitance that is 35 times that of the capacitor with no liquid

in it. Independently of the polarization, and for electric fields explored in this work, cations at both interfaces show similar orientations.

After a sudden release of the electric field, the potential difference between the electrodes decays at two different time scales: a fast relaxation process with a time constant $\tau = 0.2$ ps, and a slower process with $\tau = 8$ ps. From the analysis of the anion and cation contributions to the discharge current,it is inferred that anions play a dominant role in the relaxation. Ionic diffusion, which occurs on a much longer time scale, is not involved in the process. The study of the spectrum of charge density oscillations in the bulk suggests that the former relaxation follows a dynamics similar to that of a longitudinal optical mode in the bulk fluid.

In the context of dye-sensitized solar cells, the conclusions extracted in the present study suggest that, after photoexcitation of the dye, the negatively charged TiO_2 nanoparticles polarize the ionic liquid by repelling the anions without affecting too much the cation interfacial structure. This process of polarization buildup occurs very fast, mostly on a subpicosecond time scale, and is complete in <10 ps.

Many aspects of this process remain to be studied. For a start, a reliable estimate of the screening length within the ionic liquid is required to assess the magnitude of the electrostatic interaction between the charged nanoparticles. This aspect, which is important for a good performance of the solar cells, is difficult to assess within the present simulations where the two walls are oppositely charged. In addition, a more realistic picture of the walls that considers explicitly the TiO_2 or SiO_2 surfaces is required to describe specific aspects of the ionic liquid−solid interface, including ionic electroadsorption.

Acknowledgment. We thank Prof. P. Ballone and Dr. T. Youngs for fruitful discussions. This work was funded by the Engineering and Physical Sciences Research Council (EPSRC) of U.K., Grants GR/S41562 and EP/D029538/1. R.M.L.-B. thanks the Leverhulme Trust for an Emeritus Fellowship.

References and Notes

(1) Sakaebe, H.; Matsumoto, H. *Electrochem. Commun.* **2003**, *5*, 594−598.
(2) Nanjundiah, C.; McDevitt, S. F.; Koch, V. R. *J. Electrochem. Soc.* **1997**, *144*, 3392−3397.
(3) Grätzel, M. *Nature* **2003**, *421*, 586−587.
(4) Bockris, J. M.; Reddy, A. *Modern Electrochemistry*; Plenum Press: New York, 1988; Vol. 1.
(5) Bockris, J. M.; Reddy, A. *Modern Electrochemistry*; Plenum Press, New York, 1988; Vol. 2.
(6) Schmickler, W. *Interfacial Electrochemistry*; Oxford University Press, New York, 1996.
(7) Painter, K. R.; Ballone, P.; Tosi, M. P.; Grout, P. G; March, N. H. *Surf. Sci.* **1983**, *133*, 89−100.
(8) Ballone, P.; Pastore, G.; Tosi, M. P.; Painter, K. R.; Grout, P. G; March, N. H. *Phys. Chem. Liq.* **1984**, *13*, 269−100.
(9) Boda, D.; Henderson, D.; Chan, K. *J. Chem. Phys.* **1999**, *110*, 5346−5350.
(10) Fawcett, W. R. *Electrocatalysis*; Wiley-VCH: New York, 1998.
(11) Fawcett, W. R.; Hromadova, M.; Tsirlina, G. A.; Nazmutdinov, R. R. *J. Electroanal. Chem.* **2001**, *498*, 93−104.
(12) O'Regan, B.; Graetzel, M. *Nature* **1991**, *353*, 737−740.
(13) Grätzel, M. *J. Photochem. Photobiol. A* **2004**, *164*, 3−14.
(14) Sorensen, B. 2004. *http://mmmf.ruc.dk/energy* .
(15) Mazille, F.; Fei, Z. F.; Kuang, D. B.; Zakeeruddin, S. M.; Grätzel, M.; Dyson, P. J. *Inorg. Chem.* **2006**, *45*, 1585−1590.
(16) Kawano, R.; Watanabe, M. *Chem. Comm.* **2005**, 2107−2109.
(17) Wang, P.; Wenger, B.; Humphry-Baker, R.; Moser, J.-E.; Teuscher, J.; Kantlehner, W.; Mezger, J.; Stoyanov, E. V.; Zakeeruddin, S. M.; Grätzel, M. *J. Am. Chem. Soc.* **2005**, *127*, 6850−6856.
(18) Li, B.; Wang, L.; Kang, B.; Wang, P.; Qiu, Y. *Sol. Energy Mater. Sol. Cells* **2006**, *90*, 549−573.
(19) Lanning, O.; Madden, P. *J. Chem. Phys.* **2004**, *108*, 11069−11072.
(20) Pinilla, C.; Del Pópolo, M. G.; Lynden-Bell, R. M.; Kohanoff, J. *J. Phys. Chem. B.* **2005**, *109*, 17922−17927.
(21) Longo, C.; Paoli, M. A. D. *J. Braz. Chem. Soc.* **2003**, *14*, 889−901.
(22) Price, S. L.; Hanke, C. G.; Lynden-Bell, R. M. *Mol. Phys.* **2001**, *99* (10), 801−809.
(23) de Andrade, J.; Stassen, H. *J. Phys. Chem. B.* **2002**, *106*, 13344−13351.
(24) Barbé, C.; Arendse, F.; Comte, P.; Jirousek, M.; Lenzmann, F.; Shklover, V.; Grätzel, M. *J. Am. Ceram. Soc.* **1997**, *80* (12), 3157−3171.
(25) Nicholson, D.; Parsonage, N. G. *Computer Simulation and the Statistical Mechanics of Adsorption*; Academic Press: London, New York, 1982.
(26) Jackson, J. D. *Classical Electrodynamics;* John Wiley and Sons: New York, 1999.
(27) Forester, T. R.; Smith, W. *DL_POLY 2.0, reference manual*; 1995.
(28) Ewald, P. *Ann. Phys. Leipzig* **1921**, *64*, 253.
(29) Yeh, I.-C.; Berkowitz, M. *J. Chem. Phys.* **1999**, *111*, 3155.
(30) Kimbili, A.; Walker, A. B.; Qiu, F. L.; Fisher, A. C.; Savin, A. D.; Peter, L. M. *Physica E* **2002**, *14*, 203−209.
(31) Eppler, A. M.; Ballard, I. M.; Nelson, J. *Physica E* **2002**, 197−202.
(32) Kambe, S.; Nakade, S.; Kitamura, T.; Wada, Y.; Yanagida, S. *J. Phys. Chem. B.* **2002**, *106*, 2967−2972.
(33) Baldelli, S. *J. Phys. Chem. B* **2005**, *109*, 13049−13051.
(34) Rivera-Rubero, S.; Baldelli, S. *J. Phys. Chem. B* **2004**, *108*, 15133−15140.
(35) Bhargava, B. L.; Balasubramian, S. *J. Chem. Phys.* **2005**, *123*, 144505−144505.
(36) Triolo, A.; Russina, O.; Hardacre, C.; Nieuwenhuyzen, M.; Gonzalez, M. A.; Grimm, H. *J. Phys. Chem. B* **2005**, *109*, 22061.
(37) Del Pópolo, M. G.; Voth, G. A. *J. Phys. Chem. B* **2004**, *108*, 1744−1752.
(38) Margulis, C. J.; Stern, H. A.; Berne, B. J. *J. Phys. Chem. B* **2002**, *106*, 12017−12021.
(39) Hansen, J. P.; McDonald, I. R. *Theory of Simple Liquids*; Academic Press: London, New York, 1990.
(40) Urahata, S.; Ribeiro, M. C. C. *J. Chem. Phys.* **2006**, *124*, 074513.
(41) Hansen, J.-P.; McDonald, I. R. *Phys. Rev. A: At., Mol., Opt. Phys.* **1975**, *11*, 2111.
(42) Youngs, T. G. A. Personal communication.
(43) Yan, T.; Burnham, C. J.; Del Pópolo, M. G.; Voth, G. A. *J. Phys. Chem. B* **2004**, *108*, 11877.